Draft version March 14, 2007
Preprint typeset using LaTeX style emulateapj v. 10/09/06

EVOLUTION OF COLLISIONALLY MERGED MASSIVE STARS

Takeru K. Suzuki[1], Naohito Nakasato[2], Holger Baumgardt[3], Akihiro Ibukiyama[2], Junichiro Makino[4] & Toshi Ebisuzaki[2]

Draft version March 14, 2007

ABSTRACT

We investigate the evolution of collisionally merged stars with mass of $\sim 100M_\odot$ which might be formed in dense star clusters. We assumed that massive stars with several tens $M_\odot$ collide typically after $\sim$ 1Myr of the formation of the cluster and performed hydrodynamical simulations of several collision events. Our simulations show that after the collisions, merged stars have extended envelopes and their radii are larger than those in the thermal equilibrium states and that their interiors are He-rich because of the stellar evolution of the progenitor stars. We also found that if the mass-ratio of merging stars is far from unity, the interior of the merger product is not well mixed and the elemental abundance is not homogeneous. We then followed the evolution of these collision products by a one dimensional stellar evolution code. After an initial contraction on the Kelvin-Helmholtz (thermal adjustment) timescale ($\sim 10^{3-4}$ yr), the evolution of the merged stars traces that of single homogeneous stars with corresponding masses and abundances, while the initial contraction phase shows variations which depend on the mass ratio of the merged stars. We infer that, once runaway collisions have set in, subsequent collisions of the merged stars take place before mass loss by stellar winds becomes significant. Hence, stellar mass loss does not inhibit the formation of massive stars with mass of $\sim 1000M_\odot$.

Subject headings: globular clusters : general — stars : early type — stars : evolution

1. INTRODUCTION

Recent infrared observations of the Galactic center and the centers of other nearby galaxies have revealed a population of compact and massive star clusters located close to the centers of galaxies, such as the Arches and Quintuplet clusters (Okuda et al. 1990; Figer, McLean & Morris 1999; Figer et al. 2002), IRS 13E (Maillard et al. 2004), and IRS 16SW (Lu et al. 2005) and MGG-11 in M82 (McCrady, Gilbert, & Graham 2003). The estimated masses of these clusters are in the range of $10^4M_\odot$ to $10^5M_\odot$ while their half-mass radii are between 0.1 and 1 pc, giving rise to central densities in excess of $10^6M_\odot/pc^3$, where $M_\odot$ is the solar mass.

Dynamical simulations have also shown that if star clusters are born sufficiently compact, massive stars with $> 20M_\odot$ will sink to the cluster center within a few Myr, i.e., before the end of the stable nuclear burning phase, through dynamical friction (Portegies Zwart & McMillan 2002; Portegies Zwart et al. 2004; Freitag, Rasio & Baumgardt 2006; Freitag, Gürkan & Rasio 2006). Their stellar radii are large enough that the stars have a high chance to collide with each other after arriving at the center. N-body and Monte Carlo simulations have shown that collisions between high-mass stars in young star clusters can lead to the formation of a supermassive star with mass of several hundreds to several thousands $M_\odot$ (Portegies Zwart et al. 2004; Baumgardt et al. 2006; Freitag, Gürkan & Rasio 2006). Such supermassive stars and the intermediate-mass black holes (IMBHs) which might form out of them could be the ultra-luminous X-ray sources recently discovered by *Chandra* and HST observations (Hopman, Portegies Zwart, & Alexander 2004; Baumgardt et al. 2006; Patruno et al. 2006).

However, whether supermassive stars can really form through runaway collisions and whether IMBHs forms at the end of their lifetime is still not clear. So far, most simulations have neglected hydrodynamical processes during the collisions and the effects of stellar evolution. Stars formed from the merging of other stars might start their lives with significant abundance gradients because of incomplete mixing. In addition, since merging events happen only after a star cluster has gone into core-collapse (Portegies Zwart et al. 2004; Freitag, Gürkan & Rasio 2006), runaway stars initially have higher He abundance as a result of the nuclear burning of the parent stars. Evolution of stars formed through merging, thus, is likely to be different from the evolution of homogeneous stars with "normal" abundance.

It has been argued that the formation of IMBHs from metal-rich ($\sim$ solar abundance) massive stars is unlikely, because strong stellar winds (Kudritzki 2002; Nugis & Lamers 2000) considerably reduces the masses before the black holes form (Belkus, van Bever & Vanbeveren 2007; Yungelson 2006). However, because the lifetime of merged stars with higher He content is shorter than that of normal stars, the total mass lost during the lifetime might be smaller than these estimates.

The present paper is a first attempt towards a realistic treatment of the stellar evolution of runaway stars. In the present paper we will follow the collision of two stars by

Electronic address: stakeru@ea.c.u-tokyo.ac.jp
[1] Graduate School of Arts and Sciences, University of Tokyo, Komaba, Meguro, Tokyo, Japan, 153-8902
[2] RIKEN, 2-1 Hirosawa, Wako 351-0198, Japan
[3] AIfA, Universität Bonn, Auf dem Hügel 71, 53121 Bonn, Germany
[4] Division of Theoretical Astrophysics, National Astronomical Observatory of Japan, Mitaka, Tokyo, Japan, 181-8588

means of SPH calculations and then follow the evolution of the merger product with a stellar evolution code. The parameters of the colliding stars are taken from the results of N-body simulations of runaway merging of stars in young star clusters.

2. METHOD

Our procedure consists of three steps : (1) stellar evolution of single stars, (2) simulations of stellar collisions and (3) stellar evolution of collision products. This procedure is essentially same as that used by Sills et al. (1997, 2001). In their works, they concentrated on the formation of blue straggler stars due to the collision between low mass stars ($< 1M_\odot$). However, in the present paper we are interested in the merging process and subsequent stellar evolution in the core of a very dense star cluster where only massive stars ($> 10M_\odot$) are involved in collisions because of mass segregation.

For the second step, we perform smoothed-particle-hydrodynamical (SPH) simulations of stellar collisions with the parameters summarized in Table 1. We use a modified version of the SPH code by Nakasato & Nomoto (2003). An important modification is that we include a treatment of equation of state (EOS) of a mixture of a fully ionized ideal gas ($\gamma = 5/3$) and radiation. We adopt a modified version of Balsara type artificial viscosity (Balsara 1995; Navarro & Steinmetz 1997) with viscosity parameters $\alpha = \beta = 5/6$ as suggested by Lombardi et al. (2003). Following the results of Portegies Zwart et al. (2004), we assume that the collisions occur at $t = 1$ Myr after the formation of the star cluster, and determine the interior structure of the merged stars by calculating the stellar evolution of single stars with solar abundances (Step (1) of the procedure).

For the equal mass cases (EQ1 and EQ2 in Table 1), we use $N = 10,000$ particles for each star (mass resolution of $8.85 \times 10^{-3}\ M_\odot$). For the unequal mass cases (UE1 and UE2), we use $N = 20,000$ particles for Star 1 and $N = 6305$ for Star 2, respectively (mass resolution of $4.42 \times 10^{-3}\ M_\odot$). We assume that initially each star is separated by $2 \times (R_1 + R_2)$, where R_1 and R_2 are the stellar radii before the collision. We put the first star at the origin and the other at the x-axis with a specific tangential velocity as shown in Table 1. Larger initial velocities lead to less eccentric orbits and larger pericenter distances between the two stars and therefore longer merging times.

The SPH simulations show that the end-products of the merging events are not spherical because of their rotation (Figure 4). Indeed, the ratio between the final rotational velocity and the circular velocity at a given radius ranges between 0.2 (inner region) and 0.8 (outer region). It is not straightforward to map such a three-dimensional particle distribution into a one-dimensional profile. Even if we could map it with a scheme used by previous authors (e.g., Sills et al. 2001), implementation of rotation in a stellar evolution code is a non-trivial work. However, since the rotational energy of the merged stars is less than 15 % of the gravitational energy, rotation is not expected to affect the evolution of the stars much. In this paper we therefore neglect the effect of rotation when calculating the stellar evolution, and construct a spherical structure by simply averaging the simulation results in mass coordinate in order to handle it by a 1D spherical symmetric stellar evolution code. Also, because the SPH simulations cannot treat low density envelopes on account of limited mass resolution, we extrapolate density and temperature structure to the outer region to match the inner structure obtained by the SPH simulations. In order to do this, we adopt the Eddington approximation to derive the relation between temperature and optical depth and assume hydrostatic equilibrium to set the density structure in the outer envelopes.

	EQ1	EQ2	UE1	UE2
Star 1($M_\odot$)	88.5	88.5	88.5	88.5
Star 2($M_\odot$)	88.5	88.5	27.9	27.9
e	0.444	0.100	0.669	0.125
$V_{\rm init}$(km s^{-1})	550	700	400	650
collision time(day)	2.1	44	1.4	13
Final Mass ($M_\odot$)	165.5	156.4	106.1	98.0
$-dM(M_\odot)$ (collision)	11.5	20.6	10.3	18.4

TABLE 1
Summary of the four runs. The third and fourth lines show the orbital eccentricity e and initial tangential velocity of the stars. The last line gives the mass lost during the collisions ($-dM$).

Our stellar evolution code is based on the program originally developed by Paczynski (1970). We neglect hydrodynamical evolution and only treat evolution on a Kelvin-Helmholtz (thermal adjustment) timescale,

$$\tau_{\rm KH} \approx \frac{GM_\star^2}{2R_\star L_\star} = 10^3\ {\rm yr} \left(\frac{M_\star}{100M_\odot}\right)^2 \left(\frac{R_\star}{50R_\odot}\right)^{-1} \left(\frac{L_\star}{10^{6.5}L_\odot}\right)^{-1}, \quad (1)$$

where G is the gravitational constant, and $M_\star$ ($M_\odot$), $R_\star$ ($R_\odot$), and $L_\star$ ($L_\odot$) are stellar (solar) mass, radius, and luminosity, respectively. This is a usual procedure in stellar evolution calculations. Our code adopts the OPAL opacity (Iglesias & Rogers 1996) and equation of state (Rogers, Swenson, & Iglesias 1996) tables, and the nuclear reaction rates tabulated in Bahcall & Ulrich (1988) . We focus on the early phase of stellar evolution before the central H is exhausted. For this purpose it is reasonable to switch off nuclear burning of He and heavier elements, and to consider only H-burning because the central temperature is still not high ($< 5 \times 10^7$K in our simulations).

3. RESULTS

3.1. *SPH simulation of stellar collisions*

In all cases reported in the present work, the overall evolution is qualitatively similar: After a certain time, both stars stretch to form an extended merging product as shown in Figures 1 and 2, which depict the last phases of the merging processes for cases EQ1 and UE1 respectively. However, the mass ratio and the orbital eccentricity of the merging stars influence the details of the merging processes.

First, the mass ratio affects the material mixing in the interior of the merger products. Figure 1 shows that the material is well mixed in the equal mass case, and the elemental abundance is almost homogeneous as will be shown later. On the other hand, in the unequal mass case (Figure 2) the less massive star (Star 2), which has the

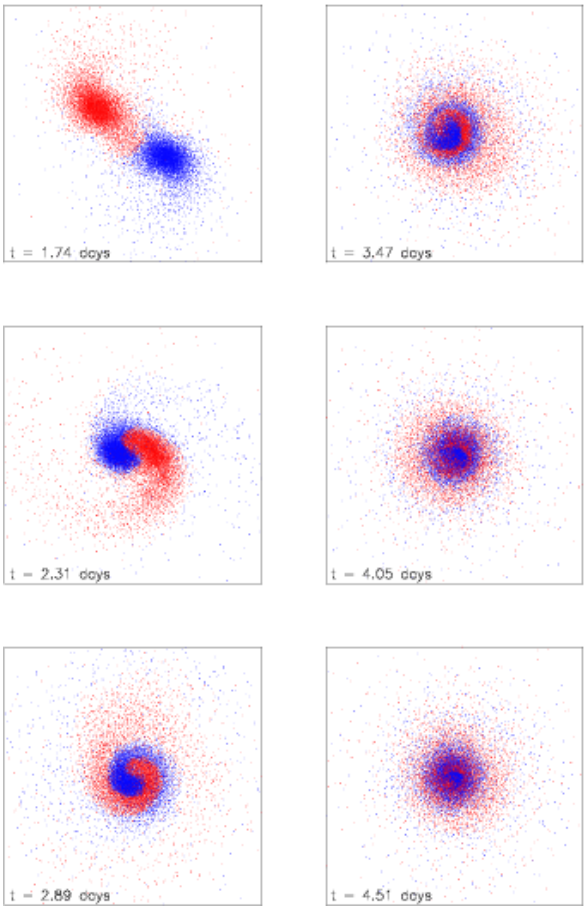

FIG. 1.— The last phase of the merging process in the SPH simulations for EQ1 case. In these snapshots, particles are projected onto the xy plane (orbital plane). The size of each panel is 100 $R_\odot$. Blue and red points represent the particles originating from Star 1 and 2, respectively.

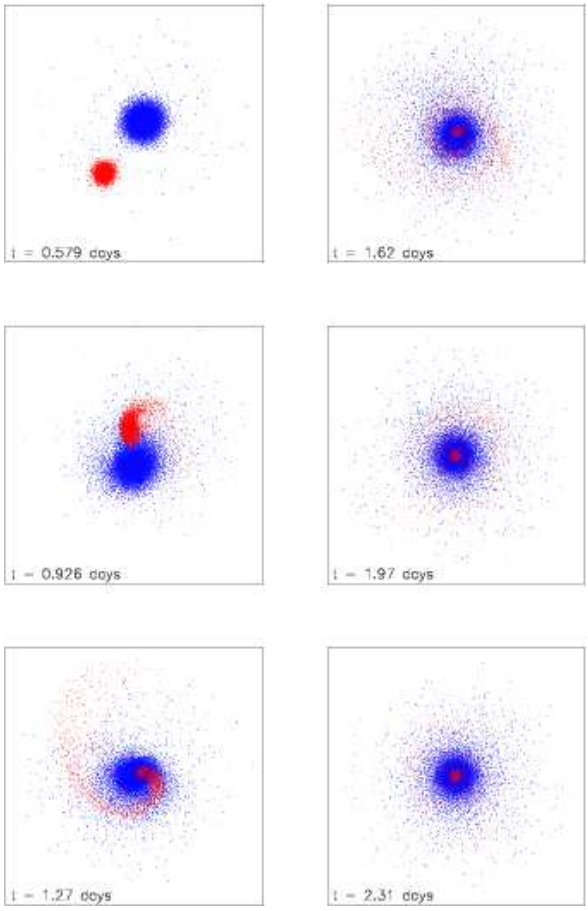

FIG. 2.— Same as Figure 1 but for UE1 case.

higher central density, sinks to the center without sufficient mixing, and the more massive star (Star 1) forms an extended envelope. As a result, the elemental abundance is also inhomogeneous in the merger product. This difference of the material mixing affects the later evolution of the merged stars, which will be discussed in §3.2.

Second, the orbital eccentricity controls the time for the stars to merge. Figure 3 shows the evolution of the distance between the centers of both stars. In a run with initially more eccentric orbit (initially smaller pericenter distance), stars merge more quickly than those in more circular orbit, mainly because the kinetic energy of the system is smaller; EQ1 takes ~ 2.1 days to merge whereas EQ2 takes ~ 44 days. EQ1 loses only 11.5 $M_\odot$ during the merging owing to the shorter collision duration, while EQ2 loses a larger mass of 20.6 $M_\odot$.

Despite the different merging time scales, the structures of the merged stars, EQ1 and EQ2, are not so different after they settle down to dynamical stable states (Figure 4). Therefore, the later evolution of the merged stars is not expected to be different between EQ1 and EQ2. We found similar tendencies in the unequal mass cases, UE1 & UE2; in UE1 with larger e, the merger product settles down to a dynamically stable state faster and the mass lost during the merger is smaller, while the later evolution is essentially the same.

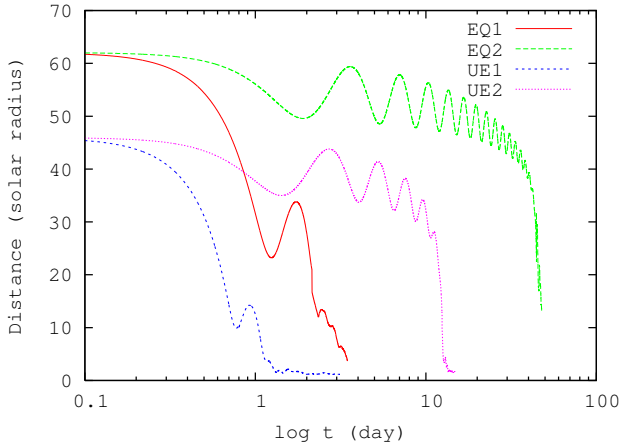

FIG. 3.— Evolution of the distance between the centers of the merging stars. In EQ1 and UE1 runs, the two stars merge after a few orbital revolutions, whereas the EQ2 and UE2 runs need much longer time to merge.

3.2. *Evolution of Collision Products*

As explained earlier, we follow the evolution of the merged stars by a 1D stellar evolution code. Since the mass ratio of the merging stars affects the structure of the merger products, and since the orbital eccentricity does not, we mainly study the evolution of EQ1 and UE1, and only briefly mention the results of EQ2 and UE2 for comparison. First, we study in detail the stellar evolu-

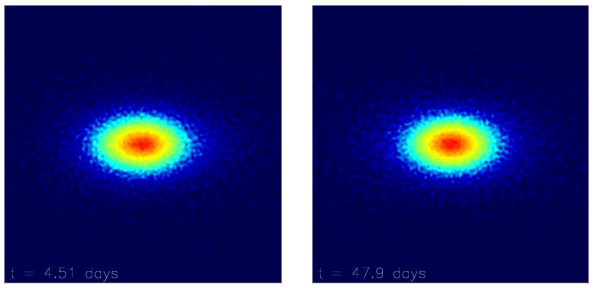

FIG. 4.— Density snapshots of the merger product at the end of the SPH simulations. Particles are projected onto the xz plane where z is the rotation axis. The size of the panels is 62 $R_\odot$. *Left* : EQ1 and *Right* EQ2

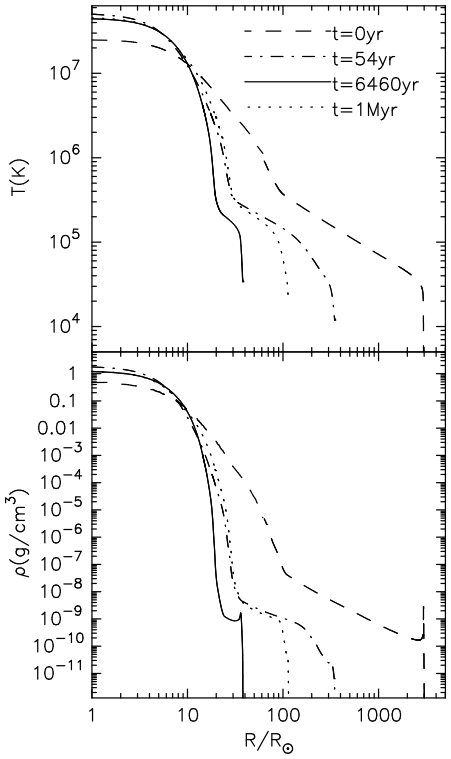

FIG. 5.— Evolution of stellar structure of EQ1. The panels show temperature (top) and density (bottom) as a function of radius in units of $R_\odot$ at $t = 0$ (dashed), 54 yrs (dot-dashed), 6460 yrs (dotted), and 1 Myr (solid) after the merging.

tion without taking into account the effect of mass loss by stellar winds. Later in §3.2.3, we present the results with mass loss for comparison.

3.2.1. *Equal Mass Collision*

Figure 5 shows the evolution of the stellar structure after the merging of the equal mass stars with large e (EQ1). The envelope is extended to $R_\star = 2960 R_\odot$, exhibiting a core-halo structure owing to the opacity peak around $T \simeq 2 \times 10^5$K (Ishii, Ueno, & Kato 1999). Because the central density and temperature are lower than those in the thermal equilibrium state at this phase, the contribution of the nuclear burning to the total luminosity is very small as shown in Figure 6. Instead, most of the energy comes from the gravitational contraction and it is transported outward by convection in the large convective core up to mass radius, $M(< R) \simeq 110 M_\odot$; the star is in a state similar to that of a pre-main sequence

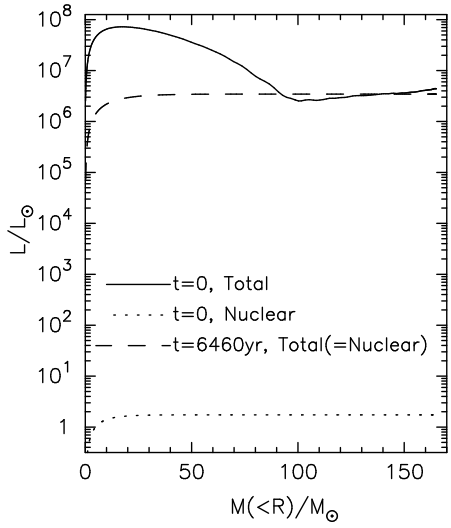

FIG. 6.— Luminosity normalized by $L_\odot$ as a function of $M(< R)/M_\odot$ for run EQ1. The solid and dotted lines give the total luminosity and the luminosity due to the nuclear burning at $t = 0$. At this stage most of the energy released comes from the gravitational contraction of the star. The dashed line shows the total luminosity at $t = 6460$, where the energy is coming from nuclear burning.

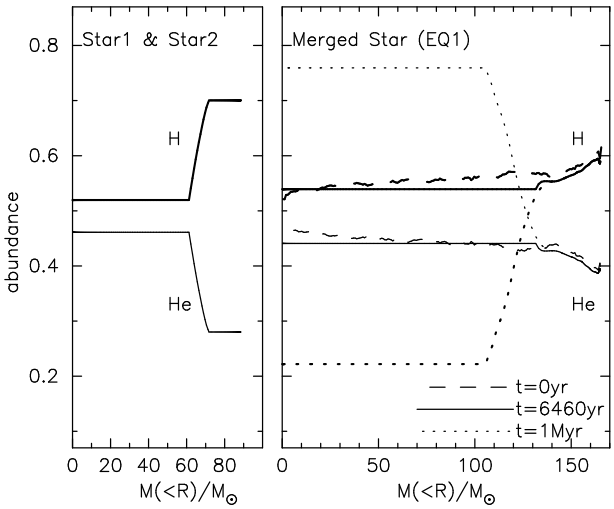

FIG. 7.— H (thick lines) and He (thin lines) abundances in the stellar interiors of EQ1. The left panel shows the abundances of Star 1 and Star 2 (both are the same in this case) just before the merger and the right panel shows the evolution of the abundances in the collision product. The horizontal axes, mass radius, $M(< R)$, in $M_\odot$ are precisely scaled in both panels. In the right panel, the dashed, solid, and dotted lines show the results at $t = 0$, 6460yr, and 1Myr.

star. The total L at $t = 0$ decreases outward between mass radii $20 < M(< R)/M_\odot < 90$. This is because the liberated energy is not converted to radiation but to internal energy, namely an increase of the temperature in this region.

Figure 7 exhibits the mass fractions of H and He in the stellar interiors. The interior is well mixed during the merger; the elemental abundance is almost homogeneous, $0.52 < X < 0.6$ and $0.46 < Y < 0.38$, even at $t = 0$ (dashed lines in the right panel), where X, Y are H and He abundances.

After the merging, the star contracts towards the thermal equilibrium state on a Kelvin-Helmholtz timescale

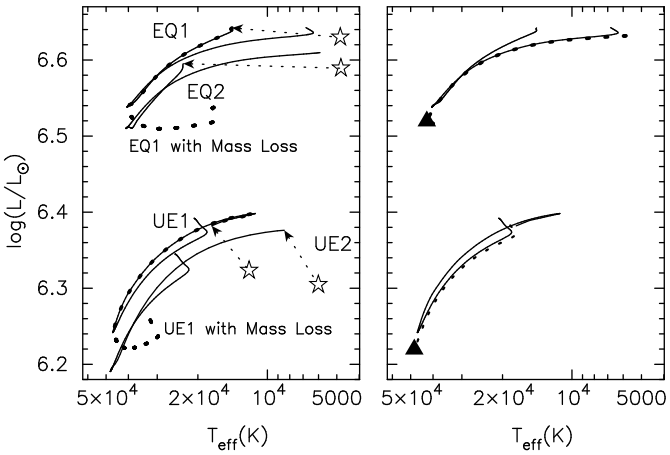

FIG. 8.— Evolution of the merged stars in a HR diagram. In the left panel, the solid lines show the results of four cases without mass loss, and the dotted lines show the results of EQ1 and UE1 with mass loss. Stars are the locations just after the merging. In the right panel the evolution of a chemically homogeneous star with $165.6M_\odot$ and $(X, Y) = (0.6, 0.38)$ and the star with $106.1M_\odot$ and $(X, Y) = (0.61, 0.37)$ are plotted (dotted lines) in comparison with the results of EQ1 and UE1 (solid). The triangles are the initial locations (zero-age main sequence) of the homogeneous stars.

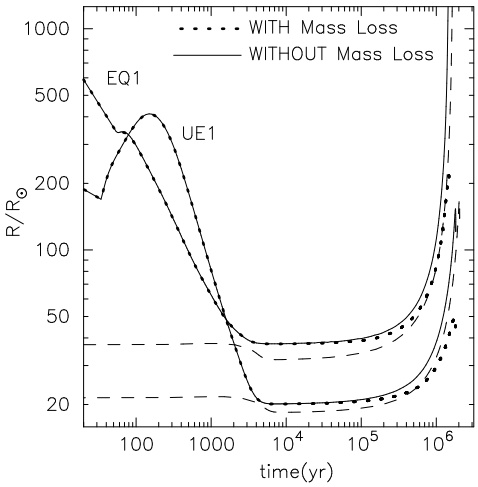

FIG. 9.— Evolution of the radii of the merged stars, EQ1 and UE1 without (solid) / with (dotted) mass loss, in comparison with the chemically homogeneous single stars (dashed) which are the same as in Figure 8.

(eq. 1). The temperature and density increase, and the convective core also grows until it occupies $\approx 80\%$ of the total mass. As a result, the elemental abundances become homogeneous inside $M(< R) \lesssim 130M_\odot$ (see the solid curves in the right panel of Figure 7). At $t = 6460$ yr after the merging, the star contracts to a minimum radius, $R_\star = 37.6R_\odot$, after which it expands gradually. At this time the star is in the stable H-burning phase, and the later evolution traces the evolution of the homogeneous single star with the same mass and similar initial abundance. These features are illustrated in Figure 8 (a Hertzsprung-Russel diagram) and Figure 9 (the evolution of the stellar radii). Due to the smaller initial H abundance, the main sequence lifetime is ≈ 1.3 Myr, which is shorter than the corresponding lifetime ($\approx$ 2Myr) of a solar abundance star with the same mass.

The evolution of EQ2 with smaller e is essentially similar to that of EQ1. Because the mass is slightly smaller,

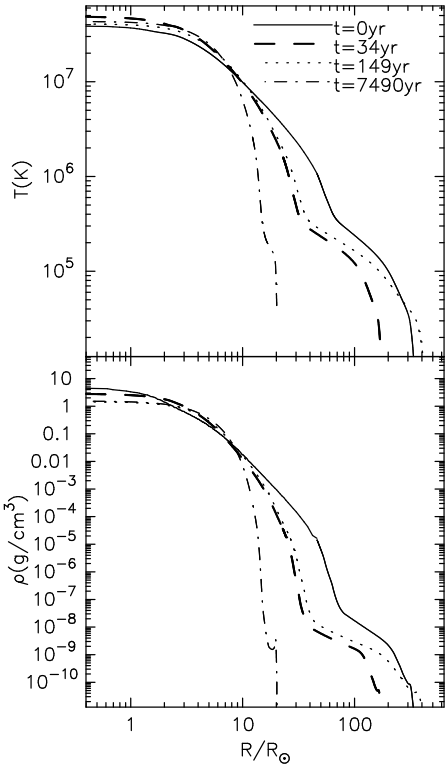

FIG. 10.— Evolution of temperature (upper panel) and density (lower panel) structure of UE1. While corresponding to Figure 5 for EQ1, this figure focuses on the initial thermal adjustment phase. The solid, dashed, dotted, and dot-dashed lines are the results at $t = 0$, 34 yr, 149 yr, and 7490 yr, respectively. Followed by the initial contraction before $t < 34$ yr, the star slightly expands between 34 yr $< t <$ 149 yr and again contracts between 149yr $< t <$ 7490 yr to the minimum radius.

the luminosity becomes lower (Figure 8). Note that $T_{\rm eff}$ of EQ2 just after the stable nuclear burning sets in (the turning point in the HR diagram) is slightly higher than that of EQ1, although the mass of EQ2 is smaller. This is because more massive stars (EQ1) have more extreme core-halo structure to show lower $T_{\rm eff}$ (Ishii et al. 1999). Chemically homogeneous zero-age main sequence (ZAMS, e.g. the triangles in Figure 8) stars of which masses exceed a certain limit also have this inverse trend. According to Ishii et al. (1999), $T_{\rm eff}$ of solar metallicity stars decreases on increasing mass in the range of stellar mass $\gtrsim 100M_\odot$, while less massive stars show the usual trend of the positive correlation between $T_{\rm eff}$ and stellar mass.

3.2.2. *Unequal Mass Collision*

The evolution of the merger products of the unequal mass stars is different from that of the equal mass cases during the initial contraction phase, while the later evolution follows chemically homogeneous stars with the corresponding masses and abundances in both cases. Figures 10 - 12 present the results of UE1, which correspond to Figures 5 - 7 for EQ1. As we have shown in §3.1, the most important difference is that the interior is not well-mixed (Figure 2). Just after the collision, the lower mass parent star (Star 2) sinks to the center without sufficient mixing because it has a higher density at the center. This star is more H-rich since the nuclear burning proceeds more slowly than in the massive partner (the right panel

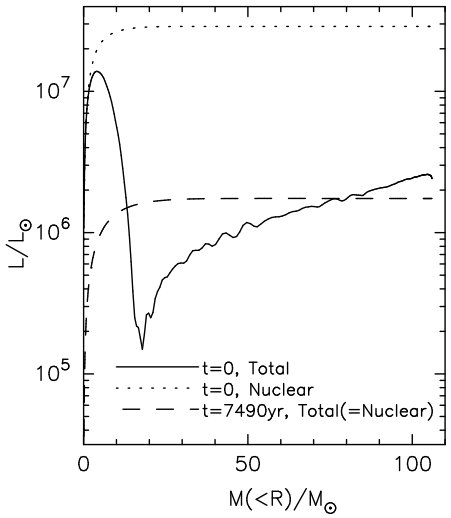

FIG. 11.— Luminosity normalized by $L_\odot$ on $M(< R)/M_\odot$ of UE1. The dotted line is the luminosity due to the nuclear burning at $t = 0$. The solid and dashed lines are the total luminosity at $t = 0$ and 7490 yr, respectively, whereas the luminosity at $t = 7490$ yr are from the nuclear energy.

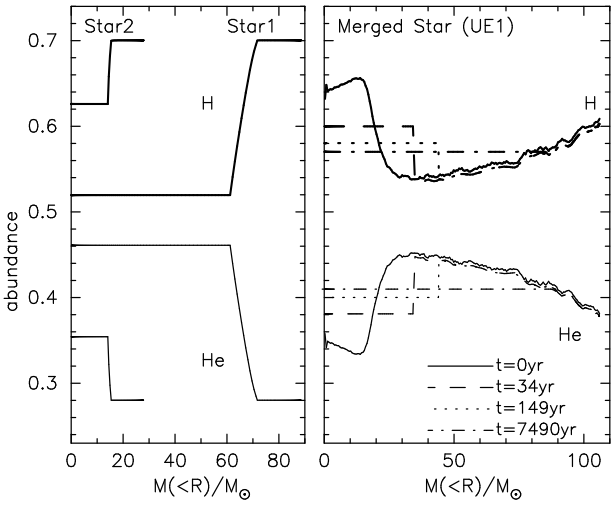

FIG. 12.— H (thick lines) and He (thin lines) abundances of UE1. The left and right panels present the results before and after the merger, and the horizontal axes are precisely scaled in both panels, which are the same as in Figure 7. In the right panel, the solid, dashed, dotted and dot-dashed lines are the results at $t = 0$, 34 yr (the local minimum of $R_\star$), 149 yr (the global maximum of $R_\star$), and 7490 yr (the global minimum of $R_\star$), respectively.

of Figure 12). Therefore, the merged star consists of a H-rich core and a He-rich outer region as shown in the right panel of Figure 12. Reflecting the higher density in Star 2, the density of the core of the collision product becomes slightly larger than the thermal equilibrium value, although the lower density envelope extends to the outer region (the lower panel of Figure 10).

Due to high density as well as moderate temperature, the nuclear burning takes place rather rapidly even just after the merging event in the unequal mass case (Figure 11). The energy release rate by the nuclear reaction exceeds the total luminosity because the nuclear energy is also used to increase the temperature (internal energy; the upper left panel) and to expand the core (work on gas, i.e., the decrease of the core density; see the lower panel of Figure 10). Accordingly, the envelope also expands from $t = 34$ yr to 149 yr (Figures 9 and 10). In fact, at $t = 149$ yr, the radius becomes, $R_\star = 412R_\odot$, which is larger than $R_\star = 337R_\odot$ just after the merger ($t = 0$). Reflecting the initial expansion, the evolutionary path in the HR diagram (Figure 8) is also more complicated compared to the equal mass case.

During this phase, the size of the convective core is small, $M(< R) < 35M_\odot$, so that the H-rich core is still preserved without mixing with the outer region (the left panel of Figure 12). In the inner region, the gradient, $\nabla \equiv \frac{\partial \ln T}{\partial \ln P}$, stays small because (i) the decrease of P with radius is rapid owing to the dense core and (ii) the decrease of T is rather slow since the core temperature is not so high, reflecting the less massive progenitor, Star 2. (Note that, in general, less massive stars have higher density and lower temperature at the centers.) As a result, the entire region outside $M(< R) = 17M_\odot$ becomes convectively stable with respect to the Schwartzschild criterion. Between $17M_\odot < M(< R) < 35M_\odot$, the gradient of mean molecular weight, μ, leads to mixing because heavier He is more abundant in the upper layer; this region is unstable only by the Ledoux criterion. Note that this is opposed to usual situations, in which heavier elements are more abundant in a lower region and μ gradient contributes to stabilization.

The initial expansion between $34 < t < 149$ yr is followed by the usual contraction to the equilibrium state through thermal adjustment. The chemical abundance becomes homogeneous from inward as the convective core grows to $M(< R) \simeq 80M_\odot$. The minimum radius, $R_\star = 20.1R_\odot$, occurs at $t = 7490$ yr, roughly corresponding to $\tau_{\rm KH}$. The later evolution traces the evolution of the single homogeneous star, which is the same as in the equal mass case. The duration of the main sequence (≈ 1.6Myr) is again shorter than the corresponding lifetime (≈ 2.5Myr) for a solar abundance star.

The evolution of UE2 is similar to the evolution of UE1: The merger product initially consists of a H-rich core and a He-rich envelope. Although this structure is maintained at first due to the small convective core, the interior becomes homogeneous after $t \gtrsim 5000$ yr as the convective core grows. The later evolution resembles the evolution of the corresponding single homogeneous star.

3.2.3. *Mass Loss by Stellar Winds*

So far we have not considered the effect of mass loss by radiation-driven stellar winds (Castor, Abbott, & Klein 1975), which also affects the evolution of the merged massive stars. The thick dotted curves in Figures 8 & 9 are the results of the evolution of EQ1 and UE1 including mass loss. Here we have adopted the mass loss rate $\dot{M}$ of solar metallicity gas from Kudritzki (2002), which tabulates $\dot{M}$ as a function of luminosity, effective temperature and metallicity[5]. Our collision products have

[5] Although in Kudritzki (2002) the dependence of $\dot{M}$ on He abundance, Y, is not explicitly presented, observation of Wolf-Rayet stars shows that $\dot{M}$ has a dependence on $\propto Y^{1.73}$ (Nugis & Lamers 2000). Our merger products are He-rich $Y \approx 0.4$ in the envelopes, compared to the Sun ($Y = 0.28$), hence, $\dot{M}$ could be be larger by a factor of 1.5-2 than that by Kudritzki (2002). However, even if $\dot{M}$ becomes larger by this extent, we suppose that the effect of the mass loss is not still crucial during the main sequence phase.

typically $\dot{M} \sim (1-3) \times 10^{-5}\ M_\odot$/yr, and, $\sim 10-30 M_\odot$ is lost during the main sequence phase of ∼1-2Myr.

Figure 8 illustrates that the luminosity becomes slightly smaller by $\approx$ 1dex at later epochs because of the mass loss. The differences of the stellar radii are not large (Figure 9); they are less than 10% except at the very end of the main sequence phase ($t \gtrsim$ 1Myr in EQ1 and $t \gtrsim$ 2Myr in UE1).

Once runaway collisions start in a dense cluster, the timescale of subsequent collisions is much shorter than 1Myr (Portegies Zwart et al. 2004). Therefore, further stellar collisions of the merged stars would take place before the mass loss becomes important in the stellar evolution. Metal-poor stars give even smaller mass loss rates than solar abundance stars. Thus, we can conclude that stellar mass loss does not stop the increase in mass due to runaway collisions, provided that the metallicity is comparable to or smaller than the solar value.

4. CONCLUSION AND PROSPECT

Bearing in mind formation of supermassive stars and IMBHs in dense star clusters, we have studied the hydrodynamical processes during collisions of massive stars and the evolution of the merger products. After the collisions, the merged stars settle down to dynamically stable states on typical timescales of days to weeks, well before they would undergo further collisions. During the merger events, the stars typically lose $\sim 10\%$ of the total mass. The merger products are He-rich because of the nuclear burning of their parent stars. The interior of the merger product of equal-mass progenitors is well-mixed during this dynamical phase. On the other hand, during the merging of unequal-mass stars, the less massive star sinks into the core, and the more massive partner is stretched to form the envelope. Since the nuclear burning took place slower in the less massive progenitor, the merged star consists of an H-rich core and an He-rich envelope.

After the merger phase, the merged stars evolve to thermal equilibrium states on Kelvin-Helmholtz timescales, 10^{3-4} yr. The evolution of the collision product of equal mass stars is very similar to a pre-main sequence star; the star monotonically contracts and the luminosity is mainly supplied from the release of gravitational energy. On the other hand, the evolution of the merger product of unequal mass stars is rather complicated due to the poorly mixed interior; the nuclear burning is already switched on owing to the sufficiently dense core, and as a result, the star slightly expands at first, which is followed by the usual contraction. During this phase, the stellar radii are still large, $\gtrsim 100 R_\odot$, so that the cross sections of stellar collisions are large. Some of merger products might undergo further collisions, if they are in dense central regions of star clusters.

After the thermal adjustment phase, the merged stars enter a stable nuclear burning phase and their evolution is well approximated by those of single homogeneous stars with corresponding masses and abundances. An important point here is that the lifetimes of merger products are shorter than solar abundance stars with the same masses because they are already He-rich from the beginning.

Our simulations show that neither mass loss during stellar collisions nor mass loss by the stellar winds prevents the growth in mass of the collision products. We can therefore anticipate that the scenario of the formation of supermassive stars by successive collisions (Ebisuzaki et al. 2001; Portegies Zwart et al. 2004) is likely to occur in realistic situations. Because of the nuclear burning, the merged stars become more H-poor. Finally, the lifetimes of massive He-rich descendants are much shorter than those of solar abundance stars with corresponding masses. We speculate that the very end-products of runaway collisions would form IMBHs quickly before suffering substantial mass loss. However, our present work does not quantitatively treat this final process. For such purpose we need to the study evolution of very massive ($\sim 1000 M_\odot$) and chemically evolved (He-rich with abundance gradient) stars. We plan to carry out such simulations in the future.

The gravity calculation of the SPH simulations has been done with reconfigurable computing board PROGRAPE-3. NN would like to thank Dr. T.Hamada for discussions and help regarding gravity calculations on PROGRAPE-3. This work is supported in part by a Grant-in-Aid for Scientific Research (18840009 : TKS) from the Ministry of Education, Culture, Sports, Science, and Technology of Japan. HB acknowledges support from the Japan Society for the Promotion of Science through Short-term visitor grant S-06709.

REFERENCES

Bahcall, J. N. & Ulrich, R. K. 1988, Rev. Mod. Phys., 60, 297
Balsara, D.S., 1995, J.Comput.Phys., 121, 357
Baumgardt, H., et al., 2006, MNRAS, 372, 467
Belkus, H., van Bever, J., Vanbeveren, D., 2007, ApJ, in press (astro-ph/0701344)
Castor, J. I. Abbott, D. C. & Klein, R. I. 1975, ApJ, 195, 157
Ebisuzaki, T. et al. 2001, ApJ, 562, L19
Figer, D.F., McLean, I.S., Morris, M., 1999, ApJ, 514, 202
Figer, D.F. et al. 2002, ApJ, 581, 258
Freitag, M., Rasio, F.A., Baumgardt, H., 2006, MNRAS, 368, 121
Freitag, M., Gürkan, M.A., Rasio, F.A., 2006, MNRAS, 368, 141
Hopman, C., Portegies Zwart, S.F., & Alexander, T., 2004, ApJ, 604, 101
Iglesias, C., A. & Rogers, F. J. 1006, ApJ, 464, 943
Ishii, M., Ueno, M., & Kato, M. 1999, PASJ, 51, 4171
Kudritzki, R.P., 2002, ApJ, 577, 389
Lombardi, Jr, J.C., et al., 2003, MNRAS, 345, 762
Lu, J.T., et al., 2005, ApJ, 625, 51
Maillard, J.P., et al., 2004, A&A, 423, 155
McCrady, N., Gilbert, A.M., & Graham, J.R., 2003, ApJ, 596, 240
Nakasato, N., & Nomoto, K., 2003, ApJ, 588, 842
Navarro, J.F., & Steinmetz, M., ApJ, 478, 13
Nugis, T., Lamers, H.J.G.L.M., A&A, 360, 227
Okuda, H., et al., 1990, ApJ, 351, 89
Paczynski, B. 1970, Acta Astronomica, 20, 47
Patruno, A., et al., 2006, MNRAS, 370, 6
Portegies Zwart, S.F., McMillan, S.L.W., 2002, ApJ, 576, 899
Portegies Zwart, S.F., Baumgardt, H., Hut, P., Makino, J., & McMillan, L. W. 2004, Nature, 428, 724
Rogers, F. J., Swenson, F. J. & Iglesias, C. A. 1996, ApJ, 456, 902
Sills, A., Lombardi, Jr., Charles D. B., Demarque, P., Rasio, F., & Sphapiro, S. L., 1997, ApJ, 487, 290
Sills, A., Faber, J., Lombardi, Jr., J.C., Rasio, F., & Warren, A., 2001, ApJ, 548, 323
Yungelson, L., 2006, contributed talk at JD05, IAU GA XXVI, astro-ph/0610021